P3.12 DIURNAL CYCLE OF SURFACE RADIATION BUDGET AND REGIONAL CLIMATE

Pamela E. Mlynczak
Science Systems and Applications, Inc., Hampton, VA

G. Louis Smith
National Institute of Aerospace, Hampton, VA

Paul W. Stackhouse, Jr.
NASA Langley Research Center, Hampton, VA

ABSTRACT

An understanding of the diurnal cycle of surface radiation is fundamental to modeling climate. For example, deep convection is initiated by the solar heating of the surface during the day, and the height to which the convection carries heat, water vapor and momentum greatly influences the resulting global circulation. The NASA/GEWEX surface radiation budget (SRB) data set is used to examine the relation of the diurnal cycles to regional climate for the average July. Over land, the net shortwave flux (SWN) at the surface provides the driving energy for the diurnal cycle of the surface temperature, which creates the diurnal cycle of the longwave upward flux (LWU). The boundary layer heating results in the cycle of longwave downward flux (LWD). The diurnal cycles of SWN, LWU and LWD over land can each be described to first order as a principal component for the time variation and a geographical coefficient, which is the empirical orthogonal function. The coefficient map is partitioned into climate classes, and a two-dimensional histogram in the domain of LWU and SWN is constructed for each class. The points cluster in different parts of the domain according to the climate class. These clusters are explained by the circulation and cloud patterns of the climate classes. For ocean, the processes are different. Since the surface skin temperature is held constant during the day-night in the SRB data set, the diurnal cycle of LWU over ocean is neglected in this study. Hence, the diurnal cycle of LWD over ocean is due to the absorption of shortwave flux within the atmosphere.

1. INTRODUCTION

The atmosphere and oceans are components of a heat engine that is driven by the absorption of solar radiation and the subsequent emission of this energy as Earth-emitted radiation. Most of the solar radiation is absorbed at the surface, raising the temperature of the surface and providing heat which is radiated as longwave upward flux (LWU); or it is transferred to the atmosphere as sensible or latent heat. The atmosphere in turn radiates longwave downward flux (LWD) back to the surface. The diurnal cycle of solar heating by net shortwave flux (SWN) drives the diurnal cycle of the atmosphere. Knowledge of the diurnal cycle of these radiation components gives insight into the many processes that are initiated.

The NASA/GEWEX Surface Radiation Budget Data Set (Gupta et al., 2004; Stackhouse et al., 2004; Cox et al., 2006) provides global coverage of the surface radiation fluxes. The data sets used in the present study are the GEWEX/SRB Release 2.5 for longwave fluxes and Release 3.0 for shortwave fluxes. The surface fluxes are based on retrievals from satellite observations of cloud cover provided by the International Satellite and Cloud Climatology Program DX data (Rossow and Schiffer, 1991) and on Goddard Earth Observing System Data Assimilation System-4 (GEOS-4) reanalysis data to describe the surface and atmospheric temperature and humidity. These fluxes are archived for a twenty-two year period from 1983 through 2005 on a quasi-equal area grid with a resolution of one degree in latitude and at the Equator one degree in longitude. Maps of fluxes are defined on GMT every three hours starting at midnight GMT.

The purpose of this paper is to compute and examine the global distribution of the diurnal cycles of SWN, LWU and LWD. The monthly-mean diurnal cycles for “all-sky” conditions are studied for July, as the strongest cycles occur in the summer and the Northern Hemisphere contains the larger fraction of land. In order to study the diurnal cycles of 64,800 regions that are required to cover the globe at one-degree equal angle resolution, a principal component analysis is used to describe the time variation over the day. These principal components (PCs) are then used to compute the geographical distribution of the strength of each PC.

Over the globe, the dominant processes in the diurnal cycles vary according to the climate class. For example, in tropical wet regions, much of the heat from the SWN is transferred to the atmosphere as latent heat, but over desert, nearly all is transferred as sensible heat. The humidity and cloud cover play an important role in determining the LWD. The relation between the diurnal cycle of each region and its climate class is also presented.

2. ANALYSIS METHOD

There are 44016 regions in the quasi-equal angle grid of the data set, each with three-hourly values for each parameter. These are regridded onto a 360° by 180° equal angle grid using replication. The first step in the analysis is to compute the mean for each term

Corresponding author address:
Pamela E. Mlynczak, SSAI, 1 Enterprise Parkway, Suite 200, Hampton, VA 23666.
E-mail: Pamela.E.Mlynczak@nasa.gov

(SWD, LWU, etc.) for each of the eight times of day for which data are given and for each grid box. For each of the eight times, the mean is computed for all days of July for all Julys in the period from 1983 through 2005.

The next step is to compute the values on the basis of local time for each grid box. For each integer hour of local time, the GMT is computed as local time minus four minutes (time) for every degree of latitude west of Greenwich. The value of each parameter is then given for local time by use of a cubic spline to interpolate between the GMT values. By using 24 local hour values based on eight, 16 dependent values are introduced. However, the results will show that the 24 values describe the diurnal cycles better than eight values can. The daily mean value is then computed and subtracted from the 24 values to form the diurnal cycle.

In order to examine the regions, principal component analysis is used. Because of the enormous thermal inertia of the ocean, the diurnal cycle over the ocean is much smaller than over land; thus land and ocean regions are treated separately. Regions with mixed land and ocean are excluded. A 24x24 covariance matrix is computed as

$$M = \Sigma\, w(x)\, D(\tau,x)\, D(\tau',x,),$$

where $D(\tau,x)$ denotes the diurnal cycle at time of day τ for region x, $w(x)$ is the area weighting for region x, and the summation is over all of the land regions x. The eigenvalues λ_i and the eigenvectors, namely the principal components $PC_i(\tau)$, of this covariance matrix are computed. The principal components describe the time variation of the diurnal cycle, and the eigenvalues provide some measure of the variation of the diurnal cycle that is explained by each PC. Finally the empirical orthogonal functions $EOF_i(x)$ provide the geographic distribution and are computed by projecting the 24 $PC_i(\tau)$ onto the 24 hourly maps for each parameter. The temporal and geographical variations of the diurnal cycle of a parameter are then given by

$$D(\tau,x) = \Sigma\, PC_i(\tau)\, EOF_i(x).$$

3. TIME AND SPACE VARIATIONS

For surface radiation budget, the downward and upward shortwave fluxes are of interest primarily to compute the SWN. The LWU is of interest because it is a measure of the heating of the surface by the SWN. Likewise, LWD is due to the heating of the planetary boundary layer PBL by the heat from the surface. These three terms, SWN, LWU and LWD, are the parameters of concern in the study of the energetics of the surface and PBL.

3.1 Diurnal Cycle over Land

Each flux is computed for each hour of the day; therefore, the diurnal cycle of each flux is described by a 24-component vector. It is convenient to use the magnitude of the vector, or equivalently the root-mean-square (RMS) of the vector, as a measure of the diurnal cycle.

Order	SWN	LWU	LWD
1	0.981	0.984	0.915
2	0.015	0.010	0.046
3	0.002	0.003	0.016
RMS	192	40.4	13.3

Table 1. Root-mean-square of surface radiation parameters (W m^{-2}) and eigenvalues (dimensionless) of principal components for land during July.

Table 1 lists the RMS of the diurnal cycle of SWN, LWU and LWD for land regions in July.

The covariance matrix for the diurnal cycle of each flux is 24x24, so that there are 24 eigenvalues. Table 1 also lists the first three eigenvalues of the covariance matrix. In each case, the eigenvalues have been normalized, divided by the trace of the covariance matrix, so that their sum is one. For SWN and LWU the first eigenvalue is greater than 0.98, and for LWD it is greater than 0.91, which means that the first PC contains most of the variance of the diurnal cycle, and very little power is left for the remaining terms. Thus the first principal component describes the diurnal cycle very well for these fluxes.

The solar heating of the surface, namely SWN, is the quantity of interest in weather and climate studies. Figure 1 shows the first four principal components for SWN as a function of local time. The mean of each PC is defined to be zero. PC-1 for SWN has a range of 500 W m^{-2}. The symmetry of PC-1 about noon shows that globally any effects of meteorology on the SWN, such as cloudiness variations from morning to afternoon, are quite small. Simplistically, the shape of PC-1 is the cosine of the solar zenith angle. However, the time of sunrise varies with latitude, so that the curve does not have a break in slope at sunrise and sunset as it would at a single latitude, but it has a continuous slope on both sides. The second principal component PC-2 for SWN is a two-wave, with maxima near the zero crossings of PC-1 and a minimum at noon. The effect of this term is to broaden or narrow the contribution of PC-1 with a change in latitude, producing longer days at high northern latitudes and shorter days at high southern latitudes. The third principal component is skew-symmetric about noon and describes the effects of morning versus afternoon cloudiness. PC-3 accounts for only 0.2% of the power in the SWN diurnal variation. However, the effects of clouds on shortwave downward flux (SWD), and therefore SWN, will vanish at sunrise and sunset. Any effects of clouds that are symmetric about noon will appear in PC-1 and -2; any effects that are skew-symmetric about noon will vanish at noon. Thus, it is not surprising that for SWN the PC-3 is small.

The geographical distribution that corresponds to PC-1 for SWN is the first empirical orthogonal function EOF-1 and is shown by Fig. 2. Insolation at the “top of the atmosphere” is a function of latitude only, so that the longitudinal variation is due to clouds. The greatest amount of sunlight at the surface is over the Sahara Desert and the deserts of the Middle East, where there are few clouds. However, because of the high albedo of these deserts, the SWN is not as high as the lower Mississippi River Basin and the mountainous western states of the U.S. because of their darker surfaces. In July, the monsoons over India reduce the SWN. Likewise, in July the deep convection zone of equatorial Africa has moved north of the Congo Basin (e.g. Bess et al., 1992), allowing high surface insolation in the Congo. The intertropical convergence zone (ITCZ) is over the south coast of West Africa. The deep convection zone of equatorial South America has moved northwest to Colombia, leaving the Amazon Basin with high surface insolation. For July, the insolation vanishes within most of the Antarctic Circle. For Greenland, the SWN is quite small due to the very high albedo of the ice cover. The EOF-2 corresponding to PC-2 is not shown but is a function primarily of latitude, describing the variation of length of day.

For LWU Table 1 shows that the RMS of the diurnal cycle is 40.4 W m^{-2} and that PC-1 describes 98.4% of the variance, overwhelming the remaining terms. Figure 3 shows the principal components for LWU. The first principal component PC-1 has a maximum value of 70 W m^{-2} and is similar in shape to that for the SWN during the day but has a definite lag of the peak value by about 1.25 hours after noon. PC-1 continues to decrease at a slow rate from sunset to sunrise to a minimum of -45 W m^{-2} so that its range is 115 W m^{-2}. Figure 4 shows the geographic distribution of this term, EOF-1, for LWU. The Sahara Desert and deserts of the Middle East have the largest diurnal cycles of LWU, followed by other deserts and steppe regions.

The second term of LWU accounts for 1% of the variance. PC-2 is a wave-2 with maxima near the zeros of PC-1 and a minimum near the peak of PC-1, so that it describes the variation of length of day with latitude. The third term for LWU describes only 0.3% of the variance. The PC-3 is a wave-1 out of phase with PC-1. The map of EOF-3 (not shown) shows artifacts due to interpolation to compute hourly values, demonstrating that the effect of the interpolation is a fraction of the 0.3% of the variance of the diurnal cycle of LWU. One advantage of the principal component method is that often the results help to separate artifacts, as in this case.

The response of the atmosphere to heating by the surface and to a lesser degree by direct absorption of solar radiation is to radiate some of that heat down to the surface. Table 1 shows that the RMS of the LWD is 13.3 W m^{-2}, about a third that of LWU and less than 4% of its global mean value.

The principal components for LWD are shown by fig. 5. The PC-1 is quite similar to that for LWU, but the peak is at 1400 LST, as the temperature of the atmosphere requires an additional time lag for its response to heating from the surface. There is a small amount of absorption of solar radiation within the air, which will be in phase with the SWN. The time response for this directly absorbed radiation is shorter than for that which is absorbed at the surface and transferred by mixing into the atmosphere. Figure 6 shows the EOF-1 for LWD. As with LWU, the largest values are over the Sahara Desert, the deserts of the Middle East and the western states of the U. S., after which the steppes are prominent. One interesting feature is that EOF-1 is quite large over the western Sahara but moderate over the eastern Sahara.

3.2 Diurnal Cycle over Ocean for July

For ocean, the diurnal cycle of temperature is small; consequently the diurnal cycle of LWU is ignored in the NASA/GEWEX SRB data set. Because of the absorption of solar radiation by the atmosphere and variations of cloud cover, there is a significant but small diurnal cycle of LWD over the oceans.

Order	SWN	LWD
1	0.989	0.728
2	0.009	0.123
3	0.001	0.060
RMS	208	3.7

Table 2. Root-mean-square of surface radiation parameters (W m^{-2}) and eigenvalues (dimensionless) of principal components for ocean during July.

Table 2 lists the RMS values for SWN and LWD over ocean. The RMS for SWN over ocean is larger than for land because of the low albedo of the ocean (0.06). The first PC of SWN describes nearly 99% of the power of this parameter. The RMS of LWD is only 3.7 W m^{-2}. Its first PC only accounts for 72% of its power, which may indicate that the diurnal cycles of LWD vary over the ocean, but because the RMS is small, the PCs are sensitive to observation errors.

Figure 7 shows the first four principal components of SWN, which are very similar to those for land. Again, the first term resembles the cosine of the solar zenith angle with rounded transitions at sunrise and sunset, and the second term provides the variation of length of day with latitude. Figure 8 shows EOF-1 for SWN. It is quite latitudinal, but the subsidence areas of the oceans appear as having strong SWN at the surface where there is little cloud cover. In July, the subsidence areas are strongest in the Northern Hemisphere.

Figure 9 shows the first four principal components for LWD over ocean. The total range of PC-1 is only 1.4% of that of SWN, and at this low level the effects of errors must be considered. Figure 10 shows the map of the first EOF of LWD. The oval at the date line is a clear artifact and is due to the lack of coverage by geostationary spacecraft. It is too far west for GOES observations and too far east for viewing by the Japanese Geosynchronous Meteorological Satellite (GMS). Likewise, there is a feature shaped like an hourglass in the neighborhood of 75^{o}E, where there is a gap between GMS and the European Meteosat. These artifacts are similar to features with which the producers and users of the ISCCP and SRB data sets are familiar. Nevertheless, in regions for which there is good coverage by the geostationary spacecraft, the results appear to have validity.

3.3 Artifacts

Every data set contains artifacts, and often the analysis of a data set will introduce artifacts. The artifacts in the SRB data set due to the Indian Ocean gap and the GMS/GOES gap were noted in regard to the EOF-1 of the LWD over ocean. These effects have been seen in a number of products using the ISCCP data set and are unavoidable given the lack of satellite coverage over those regions.

In this study, interpolating to get a data point at every hour of local solar time also has caused artifacts. These artifacts appear as features spaced at 45^{o} in longitude. They are not apparent in first order EOFs, but appear in EOF-2 for SWN over ocean. For this case, EOF-2 describes less than 1% of the variance, and the artifact is only a part of the EOF-2. Interpolation artifacts are present in the EOF-3 for LWD over ocean. For ocean, LWD EOF-3 describes less than 1 W m^{-2}, so that the effect of the artifact is negligible. Artifacts also appear in EOF-4 for every flux component, but the EOF-4 accounts for less than 1% of the variance and the effect is again negligible.

Land Climate Classes

Trewartha and Horn	NASA/GEWEX SRB
A. Tropical:	SWN > 150, LWN < 80, and RSW < 100
Tropical wet (rain forest)	Tropical and LWN < 50
Tropical wet and dry (savanna)	Tropical and LWN > 50
B. Dry:	
Desert	LWN > 105
Steppe	80 < LWN < 105
C. Subtropical	SWN > 150, LWN < 80, and RSW > 100
D. Temperate	110 < SWN < 150 and LWN < 80
E. Boreal	60 < SWN < 110 and LWN < 80
F. Polar: ice cap and tundra	0 < SWN < 60 and LWN < 80

Ocean Climate Classes

Trewartha and Horn	NASA/GEWEX SRB
A. Tropical:	SWN > 210 and RSW < 140
B. Convergence and stratus*	170 < SWN < 210 and RSW < 140
C. Subtropical	SWN > 160 and RSW > 140
D. Temperate	110 < SWN < 160
E. Polar	0 < SWN < 110

*Not a class under Trewartha and Horn.

Table 3. Climate classification by Trewartha and Horn for land and ocean and the corresponding SRB criteria. Units are W m^{-2}. SWN and LWN are annual-mean values, and RSW denotes annual range of SWN flux.

4. RELATION OF SRB DIURNAL CYCLES TO CLIMATE CLASS

Climate is closely related to surface radiation budget. On a regional basis, climate can be described in terms of climate classes. Smith et al. (2002) demonstrated that SRB could be related to climate classes as defined by Trewartha and Horn (1980) in terms of annual means and ranges of SRB fluxes. This section examines the relations between the climate classes and the diurnal cycles as measured by the EOFs of SWN, LWU and LWD. The criteria for the climate classes will first be revisited.

The criteria used by Smith et al. (2002) to relate SRB to climate class were developed using the original NASA Langley 8-year SRB data set, which had 2.5-degree resolution. It was noted that these criteria did not work as well with the NASA/GEWEX SRB Release 2.5/3.0. We modified the criteria so as to reproduce as closely as possible the climate class map of Trewartha and Horn (1980). Table 3 shows the new criteria for land and ocean. In many cases the annual mean SWN defining the boundary between land classes increased by 10 W m^{-2}. The lower boundary of the annual mean LWN increased by 10 W m^{-2} for steppe, and the lower boundary for desert increased by 15 W m^{-2}. The new climate class map is shown in Fig. 11. This figure maintains the similarity of the climate class map based on SRB to that of Trewartha and Horn (1980).

As shown in section 3, the first principal component contains most of the variance for the diurnal cycle of SWN, LWU and LWD, so that EOF-1 for each of these fluxes provides a measure of the diurnal cycle. Figure 12 shows box-whisker plots for the distribution of EOF-1 for each climate class for land during the summer; that is, results for the Northern Hemisphere are for July EOF-1 values and for the Southern Hemisphere are for January EOF-1 values. The line (whisker) indicates the range of the parameter, the box bottom and top denote the 25th and 75th percentiles, and the line across the box gives the 50th percentile. The mean is marked by the filled square in the box for the cases shown here. During the summer, the means of EOF-1 values and the box tops and bottoms for SWN increase as one looks at climate classes from the polar regions to the subtropical regions. These levels decrease for the tropical-wet regions (jungle) due to the heavy cloud cover. Likewise in summer the monsoons are present for the tropical wet/dry regions, so the EOF-1 distribution for savanna (tropical wet/dry) is very similar to that for tropical wet regions. Steppe and desert regions have SWN EOF-1 values that are comparable to subtropical regions. At mid and high latitudes, the solar declination and top of atmosphere insolation govern the climate class. At low latitudes, the solar declination does not have a large variation, and the effect of cloud cover is a major factor in determining the climate class.

For LWU the same progression is seen except for steppe and desert, which have larger EOF-1 values than the other climate classes. This is attributed to the low moisture, so that the transfer of heat from the surface in the form of latent heat is small. Thus, the surface heats up to provide the transfer as sensible heat. The LWD distributions are very similar to those for SWD and LWU. Although the EOF-1 values for LWD are comparable to those for SWN and LWU, the corresponding PC range for LWD is much smaller than those for SWN and LWU.

Figure 13 shows box-whisker plots for winter; that is, January EOF-1 values for the Northern Hemisphere and July EOF-1 values for the Southern Hemisphere. Polar regions have zero SWN, and the SWN is small into the subtropics. The distributions of EOF-1 for SWN are quite similar for savanna and tropical wet and for steppe and desert. For LWU, the diurnal cycles are small for the high latitudes. Savanna, steppe and desert have strong diurnal cycles in LWU. During winter the monsoons are gone from the savanna, which then become steppe in nature. The EOF-1 values for LWU are low for tropical wet regions, due to the high humidity and cloud cover. For LWD, the diurnal cycles are again weak for high latitudes. For savanna, tropical wet, and steppe regions, the boxes are similar, and the mean values are near 1. For LWD, the boxes from the 25th to the 75th percentiles are small, but the ranges are quite large. Steppe and desert have large ranges of SRB properties because they are determined not just by insolation but also by orography, which can limit moisture coming over the region. Although the diurnal cycles of radiation fluxes for steppe and desert are quite similar, the annual means differ, in that desert has an annual mean LWN of over 105 W m^{-2}.

The SWN drives the surface temperature and the LWU. Over land the LWD responds to the diurnal cycle of the surface heating and is related to the LWU. Figure 14 is a set of two-dimensional histograms for the LWU EOF-1 values versus the SWN EOF-1 values over land regions for the Northern Hemisphere in July. The cluster of points moves from left to right and upward as the class changes from polar through boreal to temperate. The subtropical points are within the domain covered by temperate for July. Savanna and tropical wet points are in the same area of the histogram, that is the lower part of the area covered by temperate where there are small LWU variations. As shown with the box-whisker plots, steppe and desert cover a large range of LWU variations. Next, Fig. 15 shows a set of two-dimensional histograms for the LWD EOF-1 values versus the LWU EOF-1 values, also for land regions in the Northern Hemisphere in July. The distributions here show that the EOF-1 values for LWD and LWU are fairly well correlated in each climate class, which the box-whisker plots also showed. Some of the slopes are greater than 1, which show more variability in LWD than LWU. Within temperate and steppe regions, LWU and LWD have a more one-to-one correspondence.

5. CONCLUSIONS

The diurnal cycles of surface radiation fluxes over the globe have been investigated by use of principal component analysis made using the NASA/GEWEX Surface Radiation Budget Data Set. These fluxes are net shortwave, longwave upward and longwave downward. The diurnal cycle of longwave radiation is much greater over land than over ocean due to the great thermal mass of the ocean, thus land and ocean were separated for the study. The month of July was selected as the main focus for this study, as there is more land in the Northern Hemisphere than in the Southern, and the maximum of the shortwave diurnal cycle is in July. January was also studied to provide the opposite case. The principal components describe the variation of the flux with local solar time, and maps of the corresponding empirical orthogonal functions show the geographical distributions of the diurnal cycle magnitudes.

These maps show the effects of cloudiness on surface radiation as well as the effects of solar declination and latitude. The first principal component in each case describes more than 98% of the variance, except for longwave downward flux. The asymmetries about noon are very small for shortwave fluxes, showing that globally the effects on shortwave fluxes due to cloudiness variations from morning to afternoon are small. The second principal component describes variation of length of day with latitude.

Box-whisker plots summarizing the distributions of EOF-1 values of SWN, LWU and LWD show the strengths of the diurnal cycles of these fluxes for various climate regions. In summer there is a progression of the strength of the diurnal cycles from high to low latitudes, with climate classes from polar to subtropical. Subtropical, steppe and desert regions have similar distributions of SWN. With the monsoons active in summer, savanna and tropical wet regions have similar SWN. The diurnal cycle for LWU increases from high to low latitudes, but the cycles for steppe and desert are much stronger than for other classes. For tropical wet and savanna, the diurnal cycle of LWU is small (with a mean EOF-1 value about 0.5). LWD behaves similarly to LWU.

In winter the progression of diurnal cycle strengths is not so great as in summer. However, with the monsoons not present, the cycles for SWN for savanna and tropical wet regions are stronger (EOF-1 about 1.4 in the Northern Hemisphere) than steppe and desert. Geographically the longwave diurnal cycles are largest over the Sahara and other deserts, decreasing through steppes and temperate regions and finally becoming quite small over snow-covered regions such as Greenland.

ACKNOWLEDGEMENTS

The authors gratefully acknowledge support by the Surface Radiation Budget Program from the NASA Science Mission Directorate through Langley Research Center to Science Systems and Applications Inc. and to the National Institute of Aerospace. They also acknowledge the Atmospheric Sciences Data Center of Langley Research Center for access to the NASA/GEWEX SRB data set.

REFERENCES

Bess, T. D., G. L. Smith, T. P. Charlock and F. G. Rose, 1992: Annual and interannual variations of Earth-emitted radiation based on a 10-year data set. *J. Geophys. Res.*, *Atmos.*, **97**, 12825-12835.

Cox, S. J., Stackhouse, P. W., S. K. Gupta, J. C. Mikovitz and T. Zhang, 2006: The NASA/GEWEX Surface Radiation Budget project: Overview and analysis. *Extended Abstracts, 12th Conf. on Atmospheric Radiation*, Madison, WI, Amer. Meteor. Soc., 10.1.

Gupta, S. K., P. W. Stackhouse, S. J. Cox, J. C. Mikovitz and M. Chiacchio, 2004: The NASA/GEWEX Surface Radiation Budget Data Set. *Extended Abstracts, 13th Conf. on Satellite Meteorology and Oceanography*, Norfolk, VA, Amer. Meteor. Soc., P6.6.

Rossow, W. B., and R. A. Schiffer, 1991: ISCCP cloud data products. *Bull. Amer. Meteor. Soc.*, **72**, 2-20.

Smith, G. L., A. C. Wilber, S. K. Gupta, and P. W. Stackhouse, Jr., 2002: Surface radiation budget and climate classification. *J. Climate*, **15,** 1175-1188.

Stackhouse, P. W., S. K. Gupta, S. J. Cox, J. C. Mikovitz, T. Zhang and M. Chiacchio, 2004: Twelve-year surface radiation budget data set. *GEWEX News, 14*, no. 4, 10-12.

Trewartha, G. T., and L. H. Horn, 1980: *An Introduction to Climate*, McGraw-Hill, 416 pp.

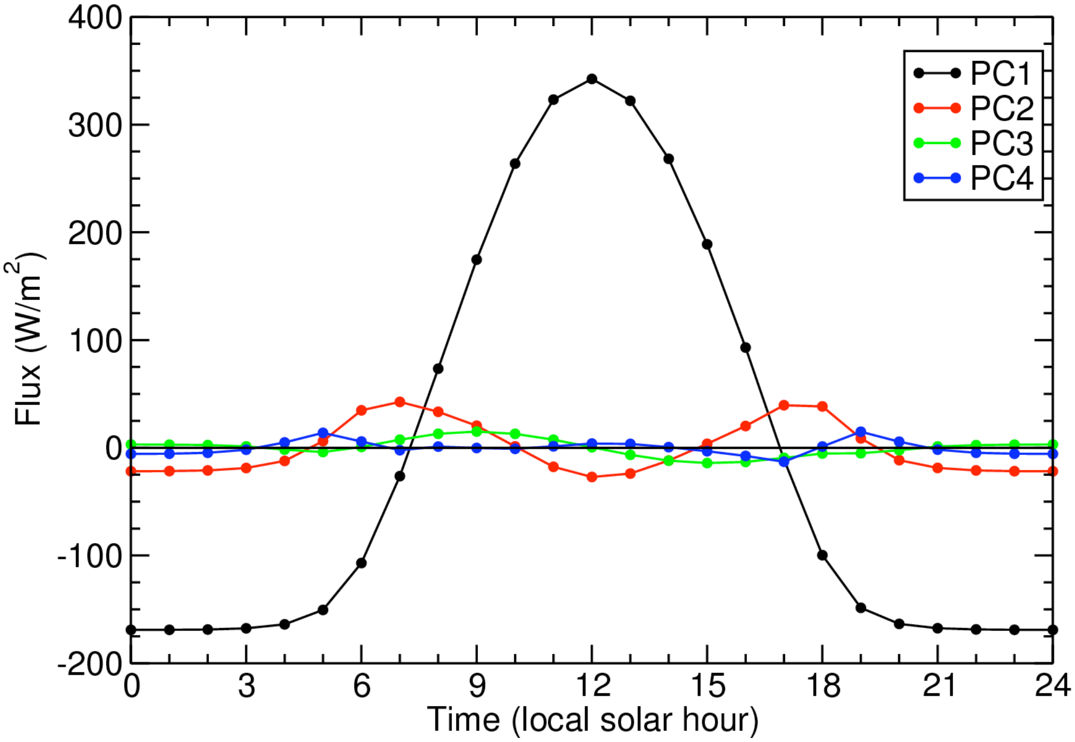

Figure 1. First four principal components of the diurnal cycle of shortwave net flux (W m^{-2}) over land in July.

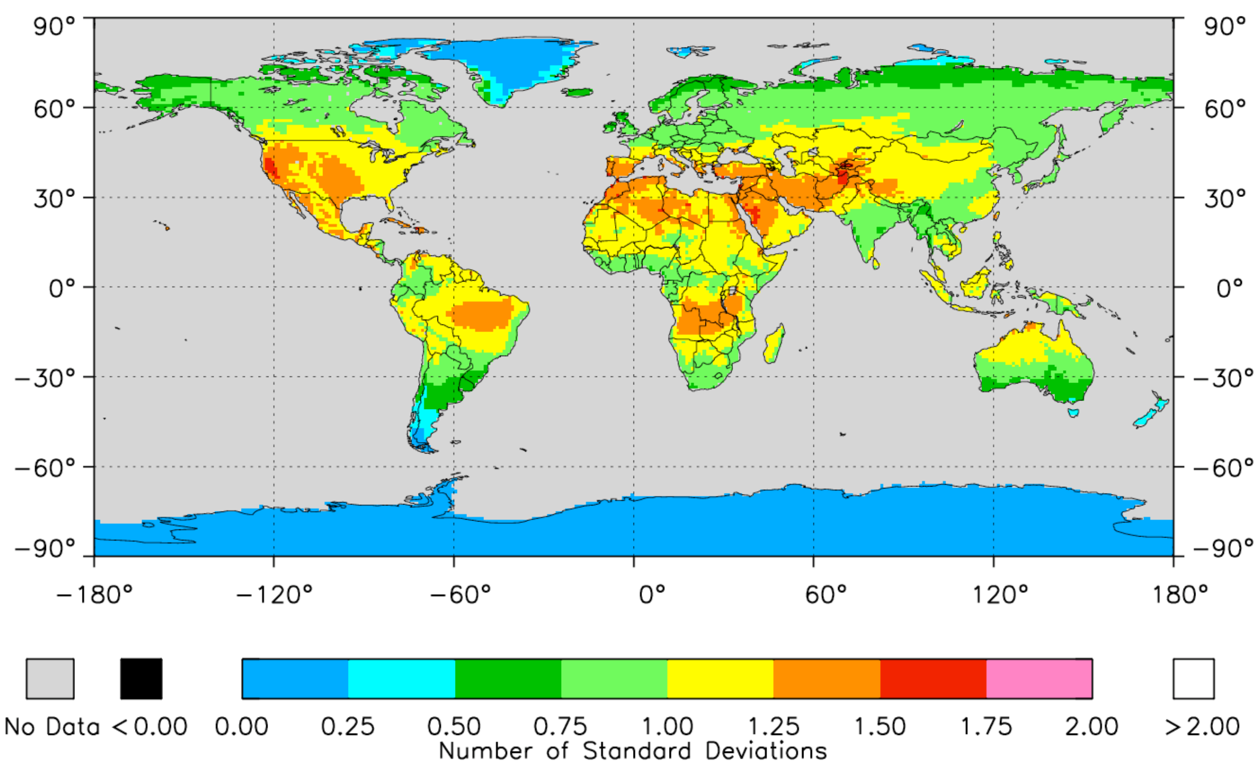

Figure 2. Map of EOF-1 of the diurnal cycle of shortwave net flux over land for July.

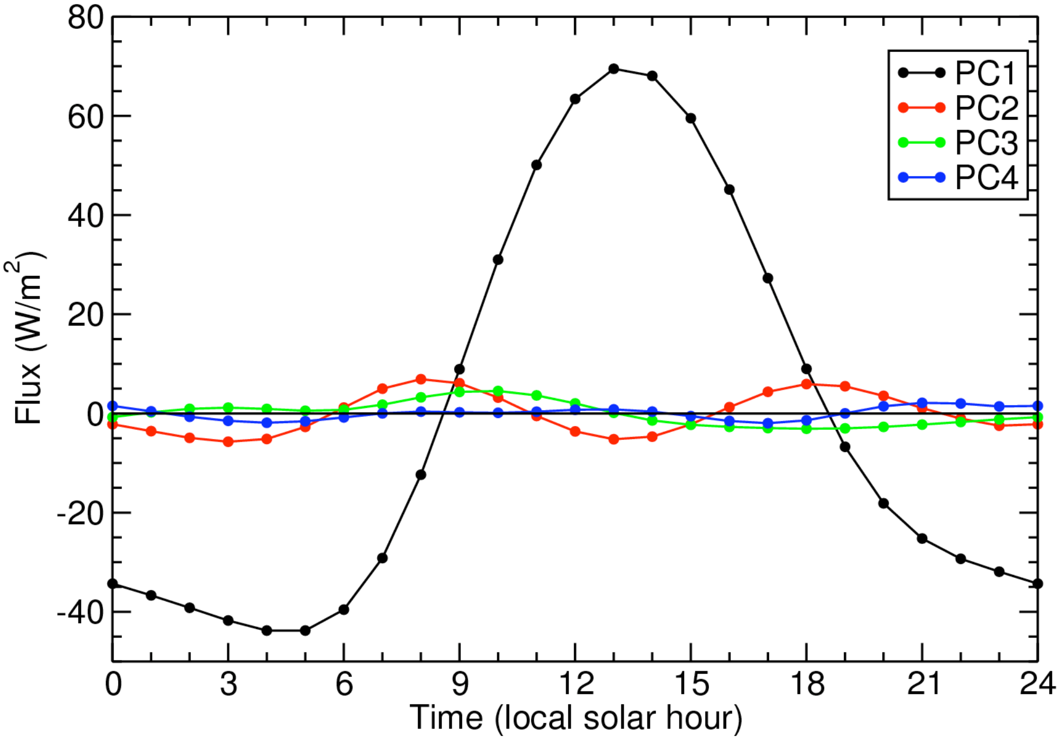

Figure 3. First four principal components of the diurnal cycle of longwave upwards flux (W m^{-2}) over land in July.

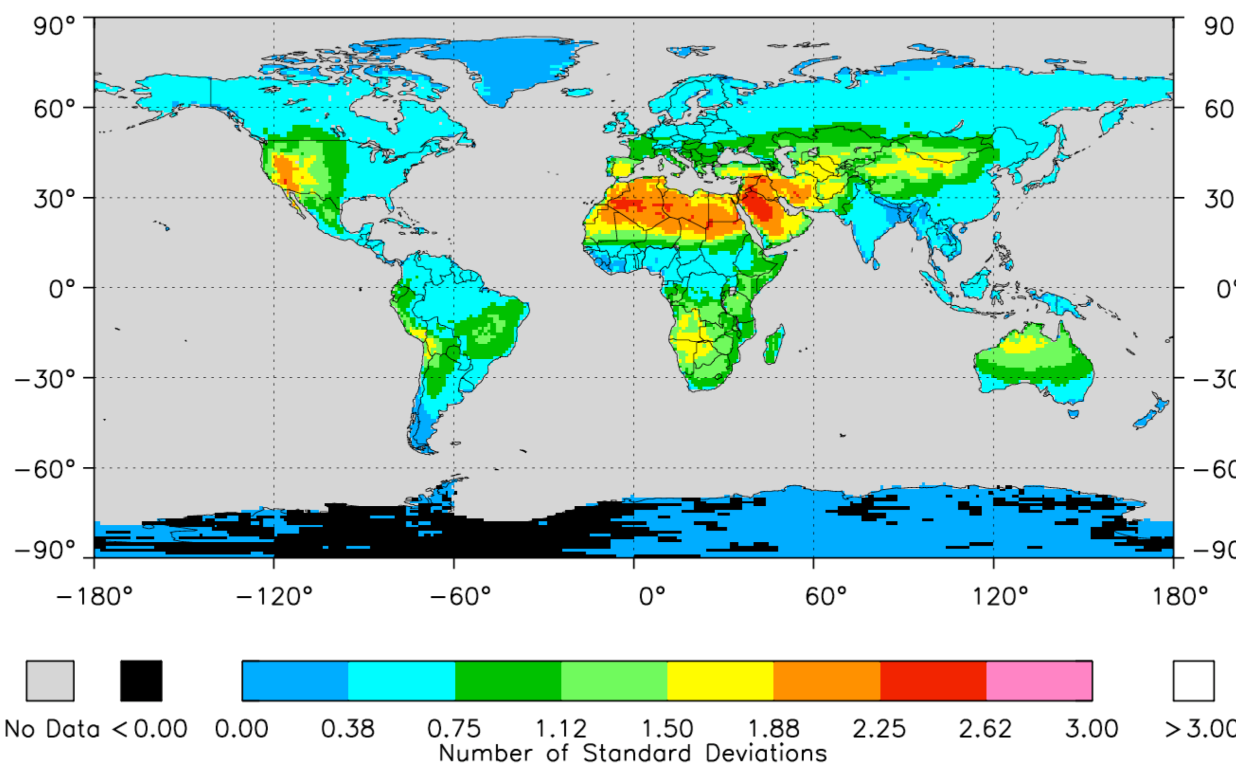

Figure 4. Map of EOF-1 of the diurnal cycle of longwave upwards flux over land for July.

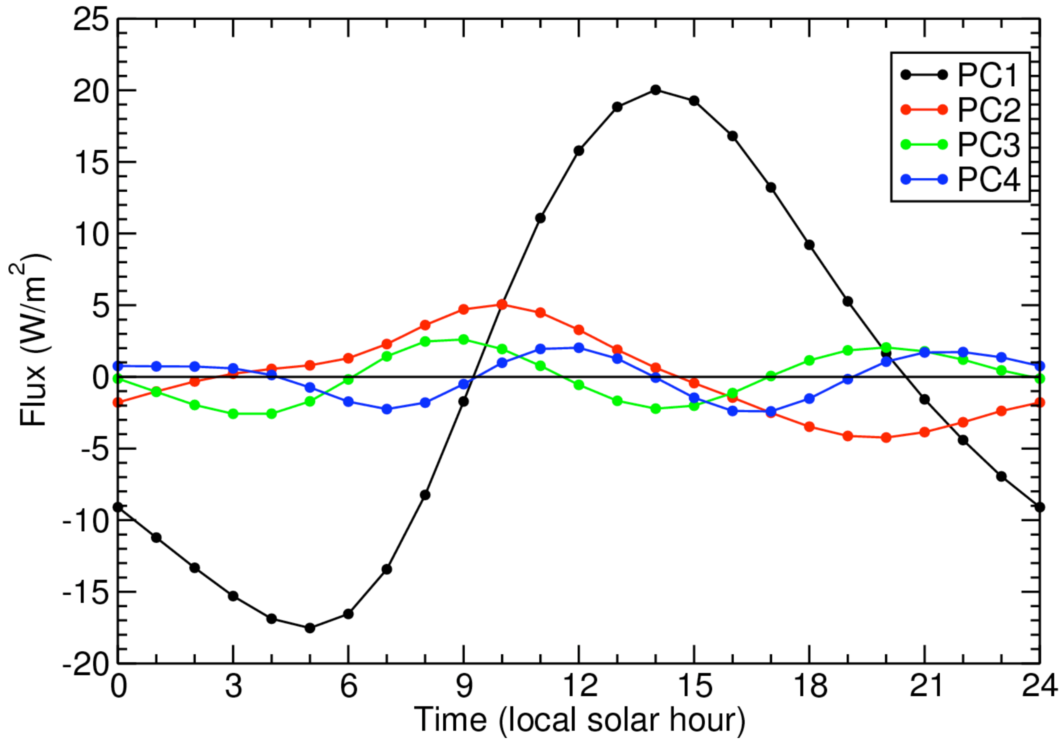

Figure 5. First four principal components of the diurnal cycle of longwave downwards flux (W m^{-2}) over land in July.

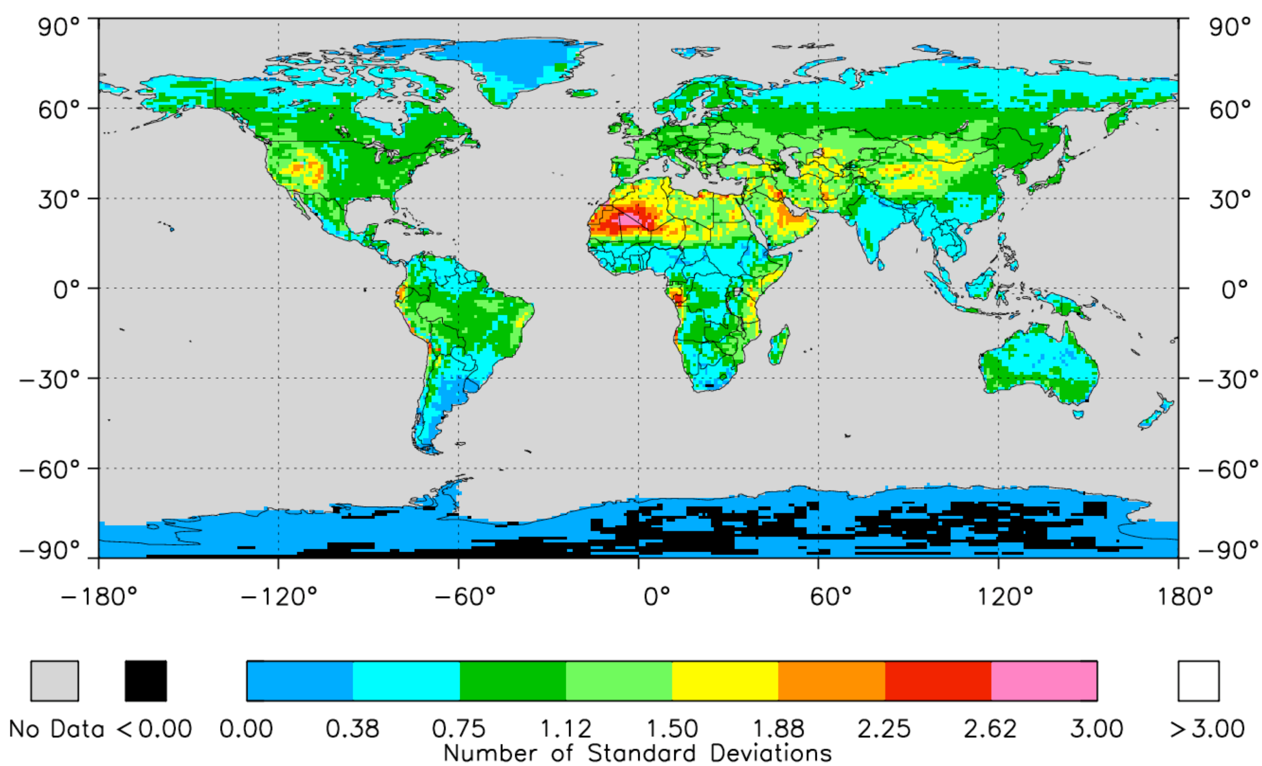

Figure 6. Map of EOF-1 of the diurnal cycle of longwave downwards flux over land for July.

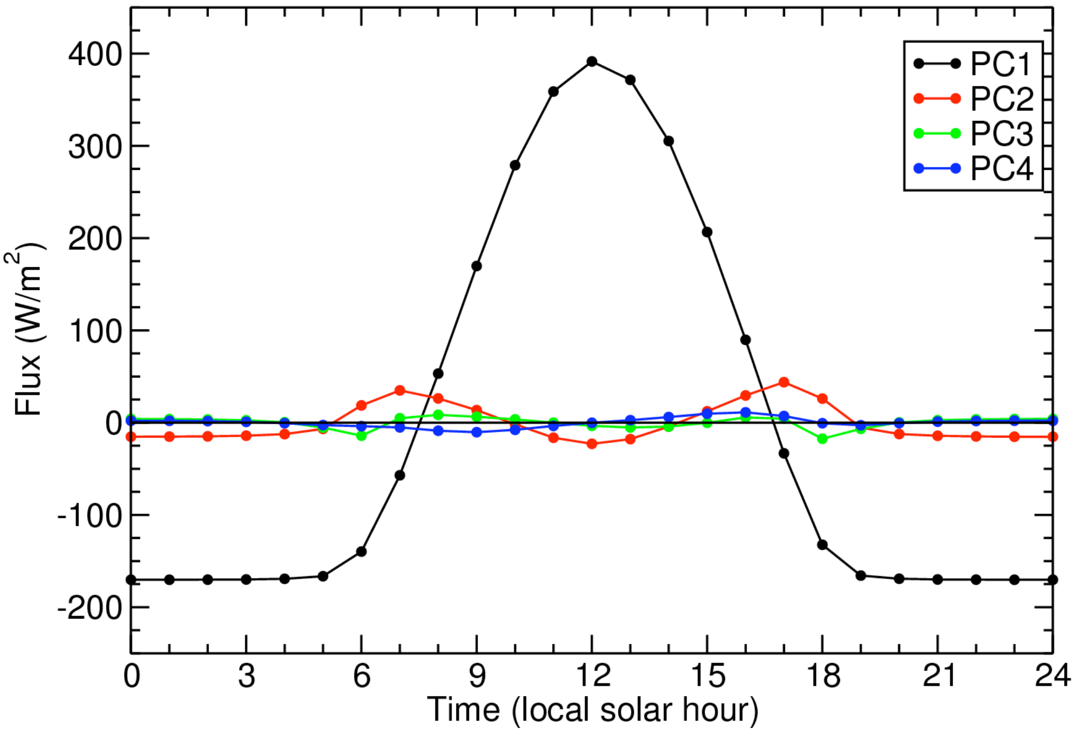

Figure 7. First four principal components of the diurnal cycle of shortwave net flux (W m^{-2}) over ocean in July.

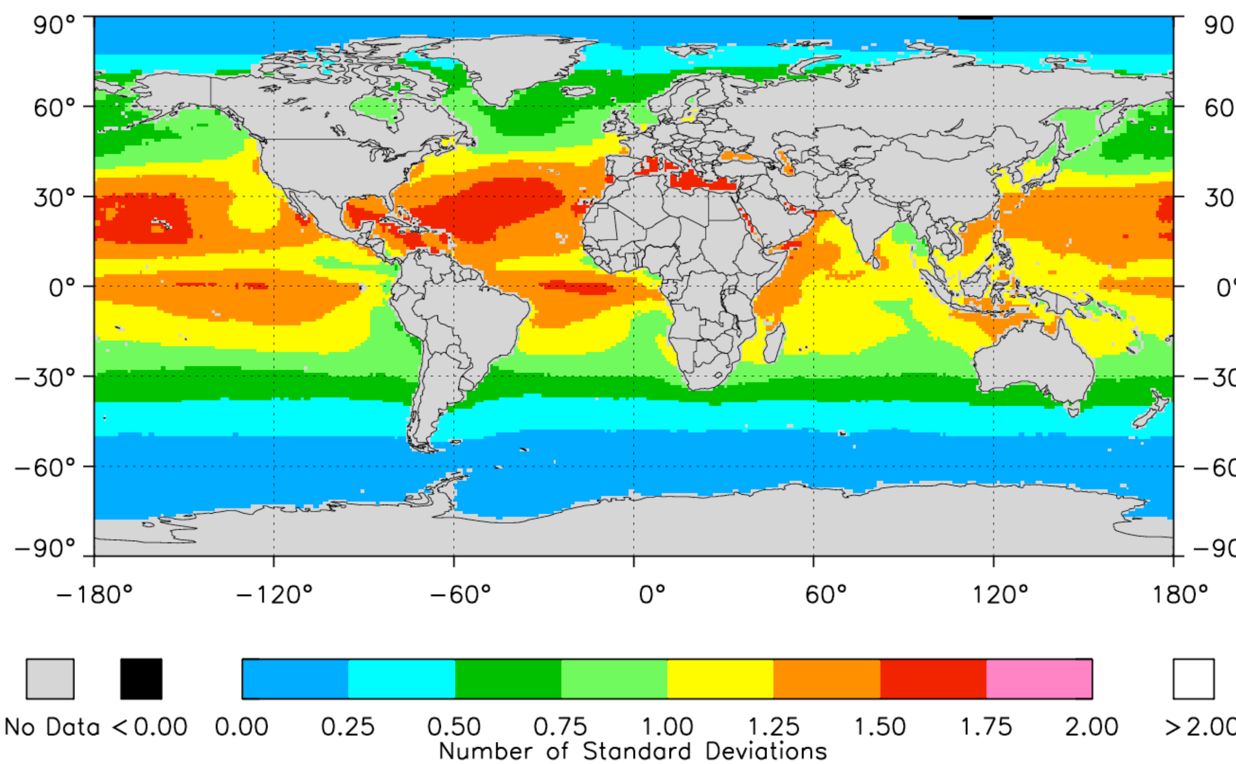

Figure 8. Map of EOF-1 of the diurnal cycle of shortwave net flux over ocean for July.

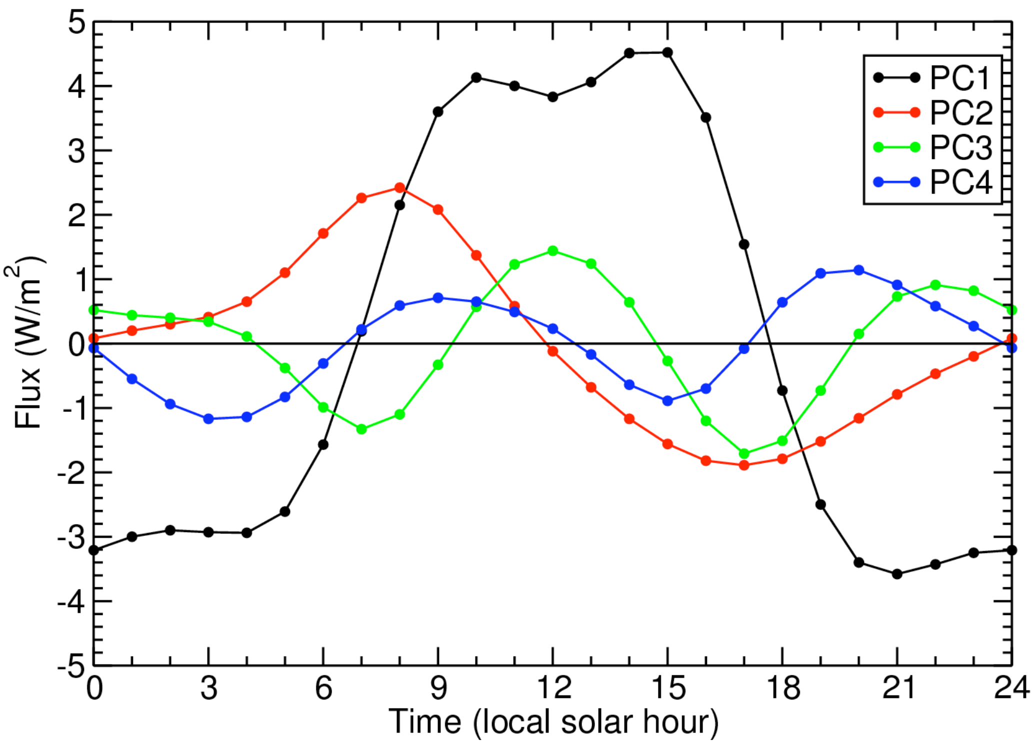

Figure 9. First four principal components of the diurnal cycle of longwave downward flux (W m^{-2}) over ocean in July.

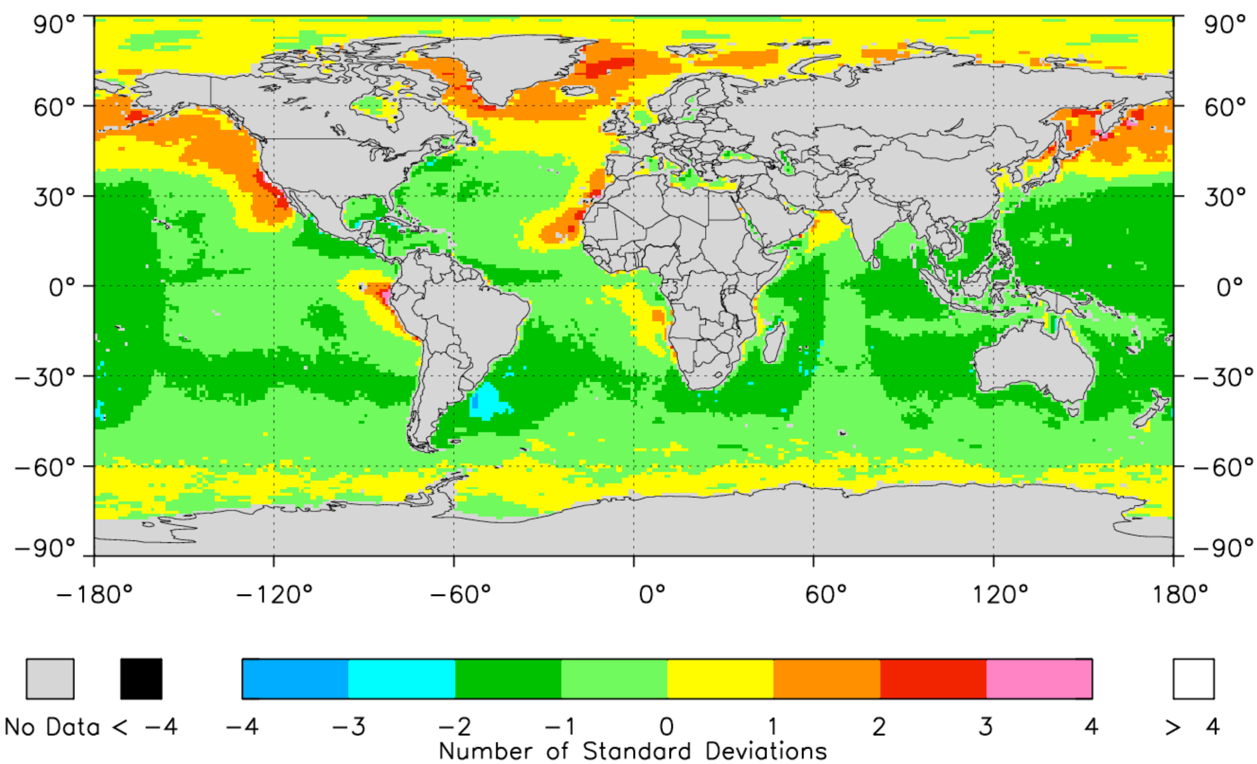

Figure 10. Map of EOF-1 of the diurnal cycle of longwave downward flux over ocean for July.

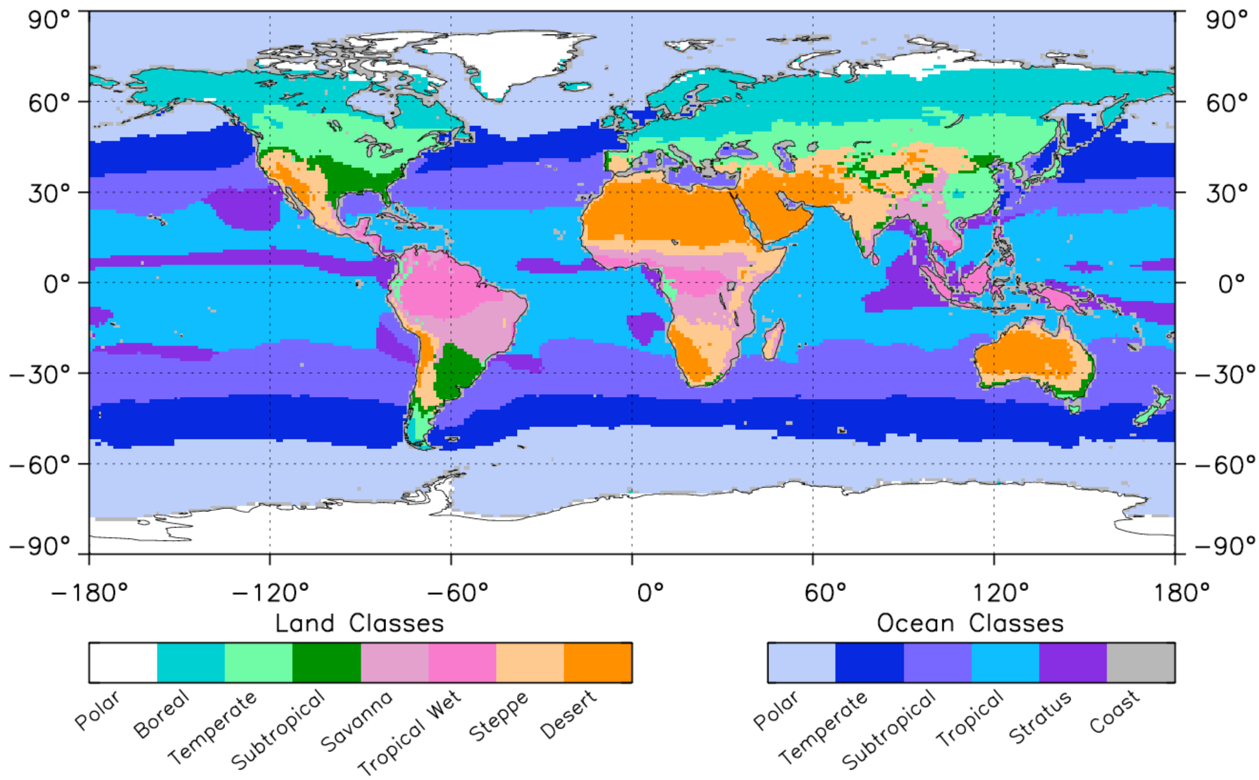

Figure 11. Map of climate classes based on Table 3 criteria.

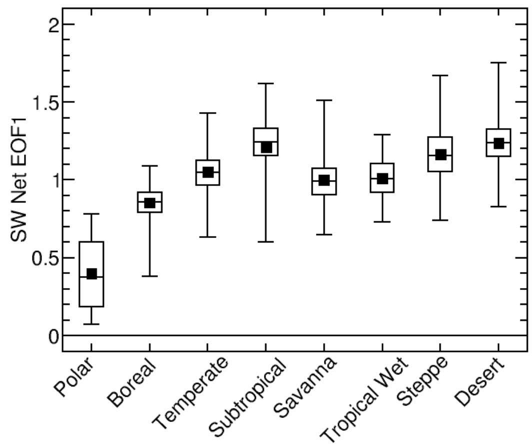

a) SW Net EOF-1 over Northern Hemisphere.

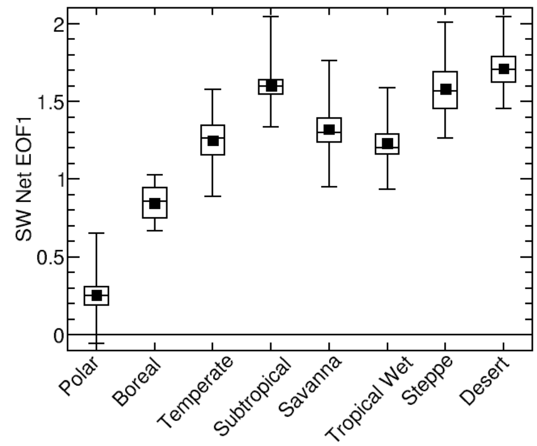

b) SW Net EOF-1 over Southern Hemisphere.

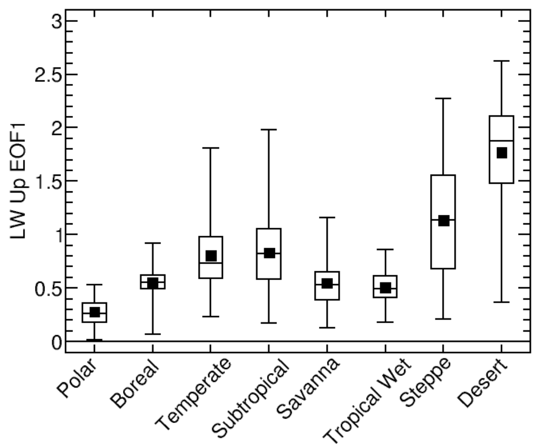

c) LW Up EOF-1 over Northern Hemisphere.

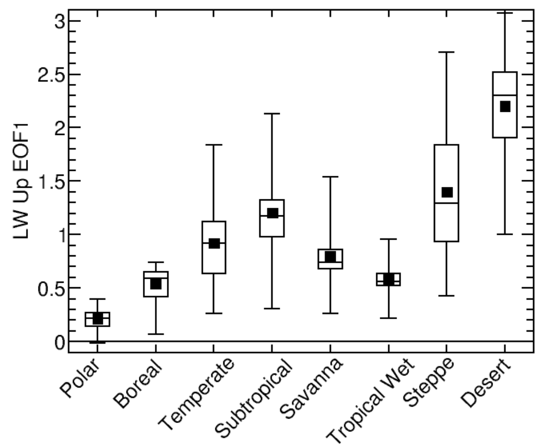

d) LW Up EOF-1 over Southern Hemisphere.

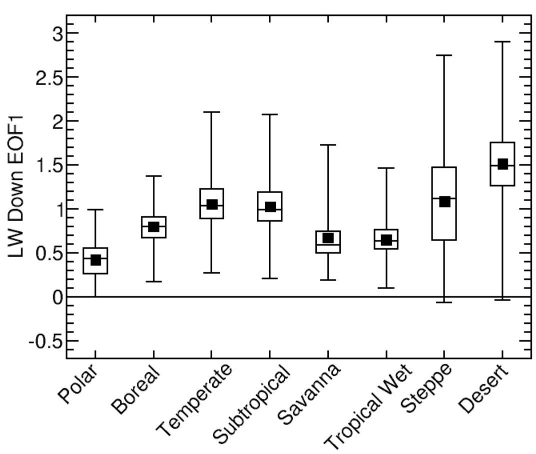

e) LW Down EOF-1 over Northern Hemisphere.

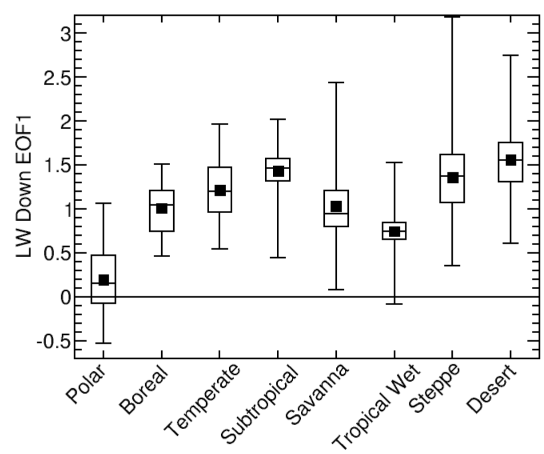

f) LW Down EOF-1 over Southern Hemisphere.

Figure 12. Box-whisker plots of EOF-1 values over land during summer, separated by hemisphere and climate class. Northern Hemisphere is for July; Southern Hemisphere is for January.

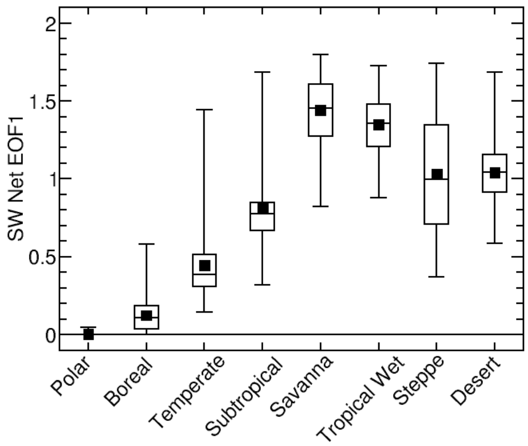

a) SW Net EOF-1 over Northern Hemisphere.

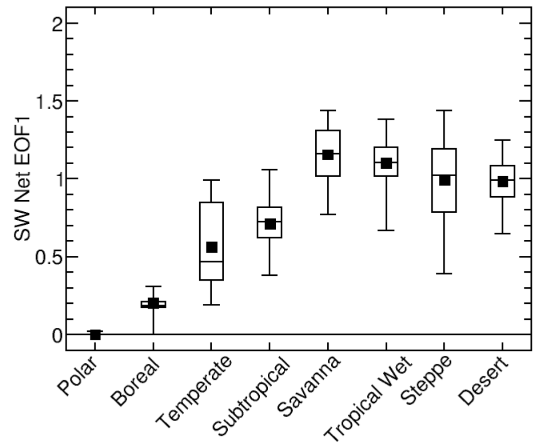

b) SW Net EOF-1 over Southern Hemisphere.

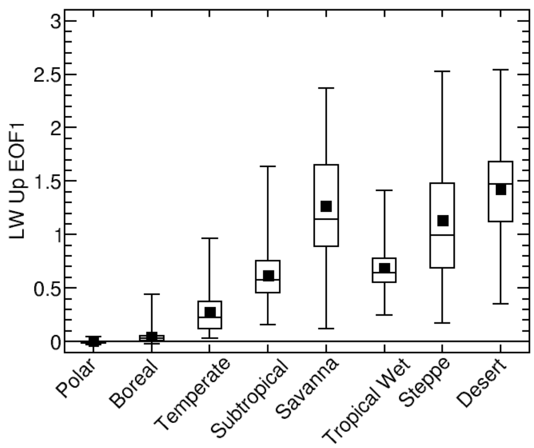

c) LW Up EOF-1 over Northern Hemisphere.

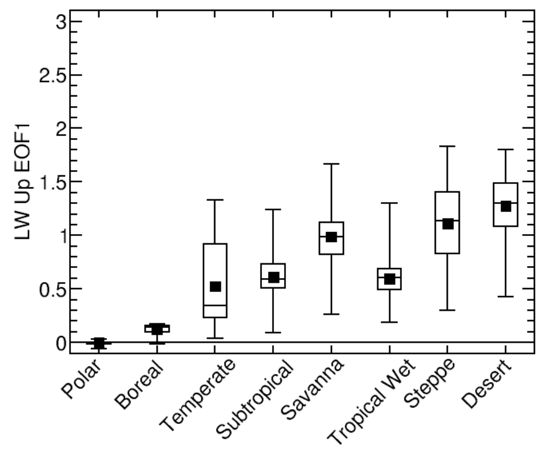

d) LW Up EOF-1 over Southern Hemisphere.

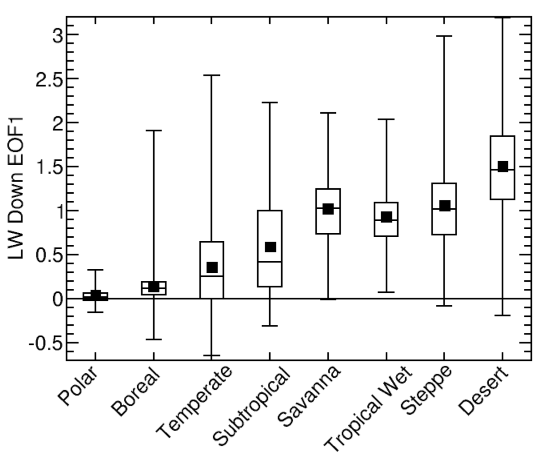

e) LW Down EOF-1 over Northern Hemisphere.

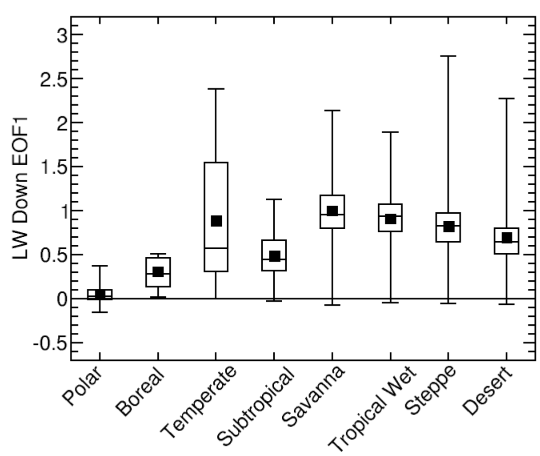

f) LW Down EOF-1 over Southern Hemisphere.

Figure 13. Box-whisker plots of EOF-1 values over land during winter, separated by hemisphere and climate class. Northern Hemisphere is for January, Southern Hemisphere is for July.

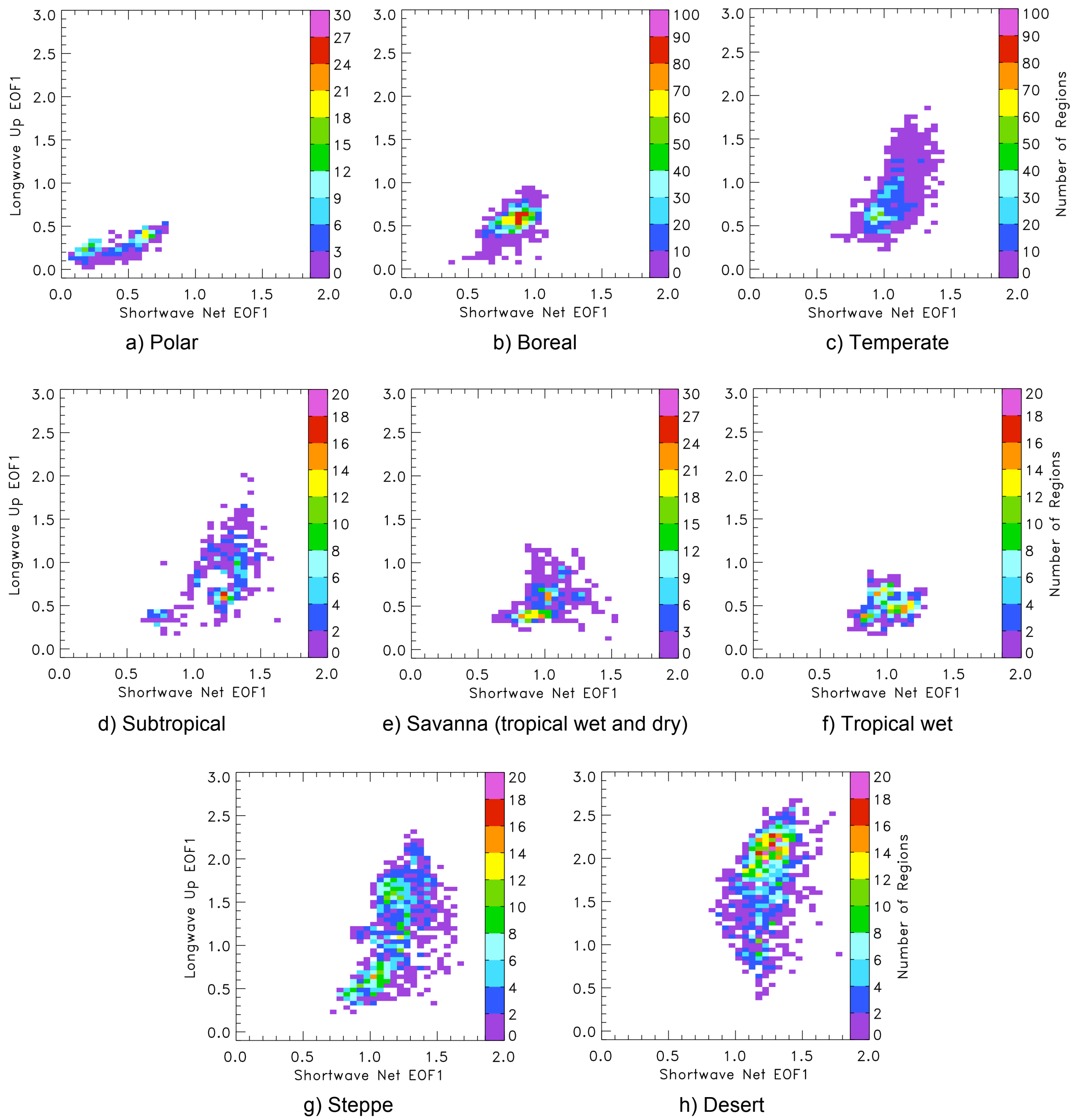

Figure 14. Two-dimensional histograms of the number of area-weighted land regions in the Northern Hemisphere as a function of longwave upward EOF-1 and shortwave net EOF-1 for each climate class.

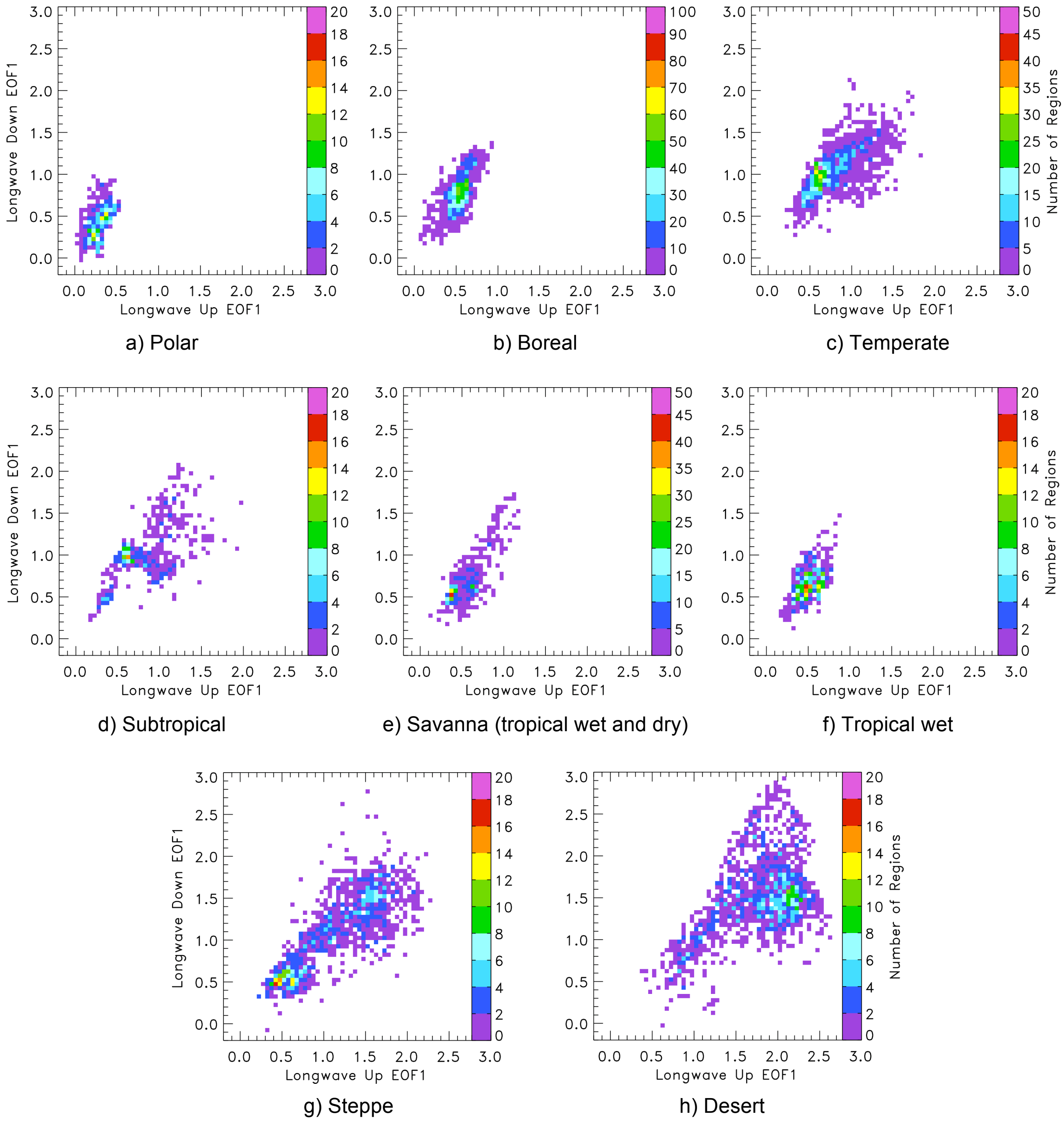

Figure 15. Two-dimensional histograms of the number of area-weighted land regions in the Northern Hemisphere as a function of longwave down EOF-1 and longwave up EOF-1 for each climate class.